Heterogeneous attenuation of sound waves in three-dimensional amorphous solids

Shivam Mahajan[1] and Massimo Pica Ciamarra [1,2,3,*]

[1]*Division of Physics and Applied Physics, School of Physical and Mathematical Sciences, Nanyang Technological University, Singapore 637371*

[2]*CNR-SPIN, Dipartimento di Scienze Fisiche, Università di Napoli Federico II, I-80126 Naples, Italy*

[3]*CNRS@CREATE LTD, 1 Create Way, 08-01 CREATE Tower, Singapore 138602*

Sound waves are attenuated as they propagate in amorphous materials. We investigate the mechanism driving sound attenuation in the Rayleigh scattering regime by resolving the dynamics of an excited phonon in time and space via numerical simulations. We find sound attenuation is spatiotemporally heterogeneous. It starts in localized regions, which identify soft regions within the material and correlate with low-frequency vibrational modes. As time progresses, the regions where sound is primarily attenuated invade the system via an apparent diffusive process.

I. INTRODUCTION

The low-frequency vibrational excitations in crystals are plane waves (phonons). On the contrary, in amorphous solids, phonons attenuate [1–5], even in the harmonic regime [6]. Sound attenuation originates from the nonaffine response [7,8] induced by amorphous solids' spatially fluctuating local elastic constants [9–15]. Some theories suggest accounting for the fluctuating elastic constants by describing an amorphous material as an elastic homogeneous medium punctuated by localized defects. If this picture holds, the scattering by these localized defects drives sound attenuation, as in Rayleigh's model [16].

Theories suggesting that sound attenuation originates from localized defects identified with quasilocalized vibrational modes (QLMs) successfully explain how the attenuation rate scales with the phonon wave vector and the stability of the material in the Rayleigh scattering regime [17]. However, they have difficulty in quantitatively relating the attenuation rate to the number of QLMs and their features [7]. One possibility is that the assumption that sound attenuation stems from localized defects is wrong, which is most likely the case in glasses that do not have a high degree of stability, and in two dimensions, where low-frequency modes are not truly localized, the number of particles involved in these modes grows with the system size [18,19]. Another possibility is that QLMs are just some of the scattering defects. In this respect, one has to consider that as the system size increases, the number of QLMs of a given frequency decreases as QLMs increasingly hybridize with plane waves.

In this paper, we establish that localized regions playing the role of defects drive sound attenuation in three-dimensional amorphous solids and show that, in small systems, these defects relate to quasilocalized vibrational modes. We investigate the nature of the attenuation process by resolving

it in space and time via the introduction of a nonphononic displacement field measuring the deviation of the particles' displacement from the phononic one. At short times, the nonphononic field is localized in a few regions, suggesting that attenuation is driven by defects. As time advances, the nonphononic field gradually spreads via a diffusive process. Mechanically soft regions may appear as anharmonic [20,21] or harmonic quasilocalized soft vibrational modes [17] (QLMs) [19,22–24] in finite-sized disorder systems. Conversely, in large systems, these soft regions are expected to be embedded within extended vibrational modes. We show that the regions where sound attenuation starts to attenuate correlate with those where QLMs concentrate and that QLMs strongly influence attenuation in poorly annealed glasses. Overall, our results indicate that scattering by defects induces phonon attenuation in three-dimensional amorphous solids and suggest that these defects emerge as QLMs in small and poorly annealed systems.

This paper is organized as follows. We introduce our three-dimensional numerical model in Sec. II and review previous work investigating the dependence of the attenuation parameter on the phonons' frequency and the material properties in Sec. III. In Sec. IV, we show that localized defects drive the attenuation of sound waves by investigating the spatiotemporal features of a nonphononic displacement field. Sections V and VI use diverse approaches to investigate how these defects correlate with quasilocalized vibrational modes. In Sec. VII, we show that the nonphononic field evolves via a diffusive process. Finally, we summarize our results and discuss future research directions in Sec. VIII.

II. NUMERICAL MODEL AND PROTOCOLS

We investigate sound attenuation in model amorphous materials that differ in their degree of mechanical stability. Particles interact via Lennard-Jones-like (LJ-like) potentials $U(r, x_c)$ that have the same repulsive part but differ in the extension of their attractive well [25], which depends on the
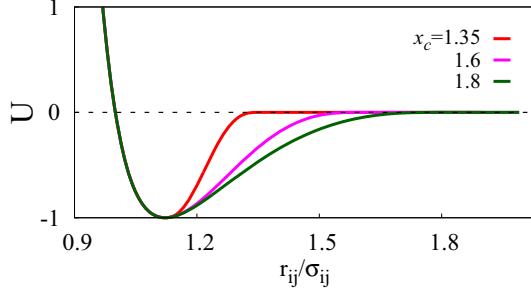
_____

*massimo@ntu.edu.sg

FIG. 1. We consider a family of LJ-like interparticle potentials that have the same repulsive part but are different in the attractive well, which extends up to $r_{ij}/\sigma_{ij} = x_c$.
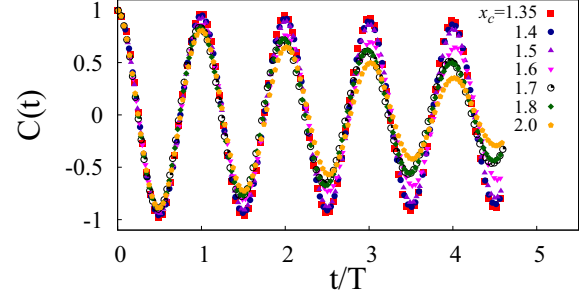

FIG. 2. Velocity autocorrelation function $C(t)$ of a transverse phonon of wave vector $\kappa = \frac{2\pi}{L}(1, 0, 0)$ for different x_c as a function of t/T, with T being the phonon's period.

parameter x_c. Examples of potentials are shown in Fig. 1. Previous works showed that x_c influences the relaxation dynamics [26] and the mechanical response [25,27–29]. In particular, the vibrational properties increasingly resemble those of stable glasses as the attraction range decreases.

We follow the model of Ref. [26] and consider polydisperse particles of diameter σ_i, drawn from a uniform random distribution in the range [0.8:1.2], in $d = 3$ spatial dimensions. The potential has a repulsive component and an attractive component. The repulsive part of the potential follows the standard LJ functional form,

$$U_r(r_{ij}) = 4\varepsilon_{ij}\left[\left(\frac{\sigma_{ij}}{r_{ij}}\right)^{12} - \left(\frac{\sigma_{ij}}{r_{ij}}\right)^{6}\right], \qquad (1)$$

where $\sigma_{ij} = (\sigma_i + \sigma_j)/2$ and acts for $r_{ij} \leqslant r_{ij}^{\min} = 2^{1/6}\sigma_{ij}$. The attractive part, which only acts for distances in the range $2^{1/6}\sigma_{ij} \leqslant r_{ij} \leqslant x_c\sigma_{ij}$, is given by

$$U_a(r_{ij}) = \varepsilon_{ij}\left[a_0\left(\frac{\sigma_{ij}}{r_{ij}}\right)^{12} - a_1\left(\frac{\sigma_{ij}}{r_{ij}}\right)^{6} + \sum_{l=0}^{3}c_{2l}\left(\frac{r_{ij}}{\sigma_{ij}}\right)^{2l}\right]. \quad (2)$$

The parameters a_0, a_1, and c_{2l} are chosen such that the potential $U(r_{ij})$ and its first two derivatives are continuous at the minimum $r_{ij}^{\min}$ and at the cutoff $r_{ij}^{(c)} = x_c\sigma_{ij}$, where the potential also vanishes. In the following, we treat m, σ, and $\varepsilon_{ij} = \varepsilon$ as the units of mass, length, and energy.

We simulate systems with $N = 64\,000$ particles in a cubic box with periodic boundary conditions at fixed number density $\rho = 1.07$. We equilibrate the systems at temperature 4.0ε, well above the glass transition temperature for the considered models [26], and then generate amorphous solid configurations by minimizing the energy via the conjugate gradient algorithm [30]. In the following, we discuss the sound-damping and vibrational properties of these amorphous configurations.

III. DEPENDENCE OF SOUND ATTENUATION ON MATERIAL PROPERTIES

We investigate sound attenuation by exciting an acoustic wave excited at time $t = 0$ [31,32] by giving each particle a velocity $\mathbf{v}_i^0 = \mathbf{A}_T \cos(\kappa \mathbf{r}_i^0)$, where $\mathbf{A}\kappa = 0$, considering κ in which two among κ_x, κ_y, and κ_z are zero and κ is the wave vector. We then evolve the system in the linear response

regime where $\dot{\mathbf{v}}_i(t) = -\sum_{j=1}^{N}\mathscr{H}_{ij}\cdot\mathbf{v}_j(t) + \dot{\mathbf{v}}_i^0\delta(t)$, with $\mathscr{H}_{ij}$ being the Hessian matrix.

The decay of the velocity autocorrelation function

$$C(t) = \frac{\sum_{i=1}^{N}\mathbf{v}_i(0)\mathbf{v}_i(t)}{\sum_{i=1}^{N}\mathbf{v}_i(0)\mathbf{v}_i(0)}, \qquad (3)$$

illustrated in Fig. 2, demonstrates phonon attenuation. A fit of $C(t)$ to a damped exponential function $\cos(\omega t)e^{-\Gamma t/2}$ allows extracting the wave-vector dependence of the attenuation rate Γ and frequency ω (or period $T = 2\pi/\omega$).

In recent work [17], we investigated how Γ depends on the phonons' frequency, system sizes, and material properties for different cutoff x_c, focusing on the low-frequency scattering regime where $\Gamma \propto \omega^4$. According to the theory of fluctuating elasticity [9,33] (FET), which assumes that the local elastic properties are δ correlated in space, Γ depends on the disorder parameter γ regulating the dependence of the fluctuations of the shear modulus on the coarse-graining size N, $\sigma^2(N)/\mu^2 = \gamma/N$, with μ being the average modulus. Specifically, FET predicts $\Gamma/\omega_0 \propto \gamma(\omega/\omega_0)^4$, with $\omega_0 = c_s/a_0$, where c_s is the sound velocity of transverse waves and $a_0 = \rho^{-1/d}$, with ρ being the number density. An extension of FET [34], which we termed correlated fluctuating elasticity (corr-FET), considers the influence of the shear modulus's spatial correlation length ξ. If $\gamma \propto (\xi/a_0)^3$, as we observed [17] and expected if the disorder parameter is proportional to the correlation volume of the shear modulus, then corr-FET predicts $\Gamma/\omega_0 \propto \xi^3\gamma(\omega/\omega_0)^4 \propto \gamma^2(\omega/\omega_0)^4$. Our previous investigation, summarized in Fig. 3, indicates sound attenuation is described by corr-FET rather than by FET, indicating the shear modulus's correlation length scale ξ changes with x_c. We found the same result holds for a different three-dimensional model. These three-dimensional results vary from those of previous investigations of two-dimensional systems, in which FET appeared to hold [15] and sound attenuation in the Rayleigh regime did not correlate with localized defects [35].

Interestingly, Rayleigh's [16] original model, according to which the scattering by localized defects drives sound attenuation, reproduces corr-FET's prediction provided the defects satisfy some conditions. While we gave indirect evidence suggesting that these conditions are met and that the scattering defects promoting sound attenuation are the quasilocalized vibrational modes, the relevance of the defect's picture remains
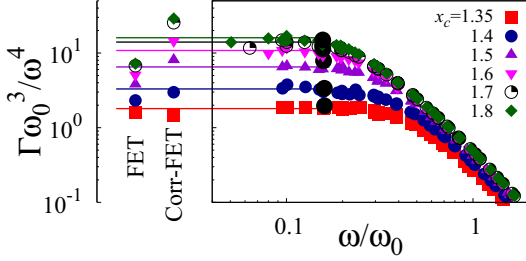
FIG. 3. Dependence of the scaled attenuation rate on the scaled frequency. The plot combines data for $N = 32\,000$, $64\,000$, $256\,000$, $512\,000$, $2\,048\,000$ and $8\,192\,000$, for which no size effects are apparent. Symbols refer to different interaction potentials as in Fig. 2. In the Rayleigh scattering regime, the correlated version of the fluctuating elasticity theory accounts for the dependence of the attenuation rate on the material properties. In this paper, we resolve in space and time the evolution of low-frequency phonons with wave number $n = 1$ in systems of $N = 64\,000$ particles, as indicated by the black circles and squares. Adapted from Ref. [17].

controversial [7]. We investigate this issue by resolving the damping of the phonons in time and space.

IV. LOCALIZED DEFECTS PROMOTE SOUND ATTENUATION

To unveil the microscopic mechanism driving sound attenuation, we spatially resolve the time evolution of the excited transverse phonons by introducing a nonphononic displacement field

$$\mathbf{dr}_i^{\mathrm{np}}(t) = \mathbf{dr}_i(t) - \mathbf{dr}_i^{\mathrm{ph}}(t), \tag{4}$$

where $\mathbf{dr}_i(t)$ is the displacement of particle i and $\mathbf{dr}_i^{\mathrm{ph}}(t)$ is the phononic displacement it would have in the absence of attenuation,

$$\mathbf{dr}_i^{\mathrm{ph}}(t) = -\frac{\mathbf{A}}{\omega}\sin(\kappa\mathbf{r_i} - \omega t + \phi) + \frac{\mathbf{A}}{\omega}\sin(\kappa\mathbf{r_i} + \phi), \tag{5}$$

with $\mathbf{A}$ being the polarization vector, κ being the wave vector, $\omega = c_s\kappa$, dt being the integration time step, ϕ being a phase, and c_s being the shear wave speed.

We filter out the influence of the slow-varying phononic field on the nonphononic displacement by studying it at stroboscopic times sT, with T being the period. We further compare $\mathbf{dr}_i^{\mathrm{np}}(sT)$ to its value at the relaxation time $s_\tau T$, with s_τ being the smallest integer ensuring $s_\tau T = \tau = \leqslant 2\Gamma^{-1}$. This comparison leads to the introduction of a local time-dependent sound attenuation parameter

$$\Delta_i^2(sT) = \frac{\langle|\mathbf{dr}_i^{\mathrm{np}}(sT)|^2\rangle}{\langle|\mathbf{dr}_i^{\mathrm{np}}(\tau)|^2\rangle}, \tag{6}$$

which is defined for $sT \leqslant \tau$. Here, $\langle\cdot\rangle$ indicates an average are over phonons with different phases in $\phi \in [0, \pi/2]$ and the same $n^2 = n_x^2 + n_y^2 + n_z^2$, where $\kappa = \frac{2\pi}{L}(n_x, n_y, n_z)$.

We have investigated the local sound attenuation parameter induced by different long-wavelength phonons. We focus on the Rayleigh scattering regime by considering the longest-wavelength phonons ($n^2 = 1$; circles in Fig. 3). We average $\Delta_i^2(t)$ over 30 phonons differing in polarization or phase.
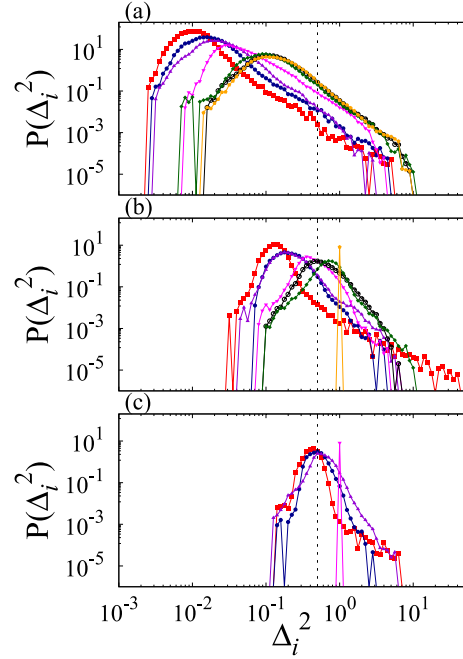

FIG. 4. Probability distribution of the local sound attenuation parameter Δ^2 at times corresponding to (a) one, (b) four, and (c) eight phonon oscillation periods. Symbols identify different interaction potentials, as in Fig. 2. We restrict the analysis to times $\leqslant 2\Gamma^{-1}$ and hence do not show data for large x_c values in (c). The vertical dashed line marks the threshold Δ_c^2 used to identify the particles with a large value of the attenuation parameter.

Figure 4(a) illustrates the probability distribution of Δ_i^2 for the different interaction potentials at a time corresponding to one period of oscillation. The displacement is close to the expected phononic one for most particles, $\Delta_i^2 \ll 1$. However, the distributions have extended right tails, indicating the existence of a few particles whose motion strongly differs from the phononic one. As time advances, the distribution's peak shifts towards $\Delta_i^2 = 1$, and the variance decreases, which is apparent from Figs. 4(b) and 4(c), which illustrate $P(\Delta_i^2)$ after four and eight oscillation periods. At the relaxation time, the distribution becomes $\delta(\Delta_i^2 - 1)$. This occurs in Fig. 4(b) for $x_c = 2$ [$\tau(x_c = 2) = 4T$] and in Fig. 4(c) for $x_c = 1.6$ [$\tau(x_c = 1.6) = 8T$].

The particles with local attenuation parameter $\Delta_i^2(t)$ larger than a threshold Δ_c^2 identify the spatial region where sound attenuated. The threshold Δ_c^2 should be large enough to select as attenuated only the particles in the tail of the $P(\Delta_i^2)$ distribution at early times. It should also be smaller than 1, the value of $\Delta_i^2(t)$ at the relaxation time. We have checked that the choice of Δ_c^2 is not critical as long as the above conditions are met and fixed in the following $\Delta_c^2 = 0.5$.

We illustrate in Fig. 5 (left column) the particles with $\Delta_i^2(t) > \Delta_c^2$ at a time corresponding to one phonon period. Different rows correspond to different interaction potentials, with the attraction range increasing from top to bottom. The field is localized in compact clusters whose typical size increases with the attraction range, i.e., as the system becomes less stable. Overall, this simple investigation unambiguously
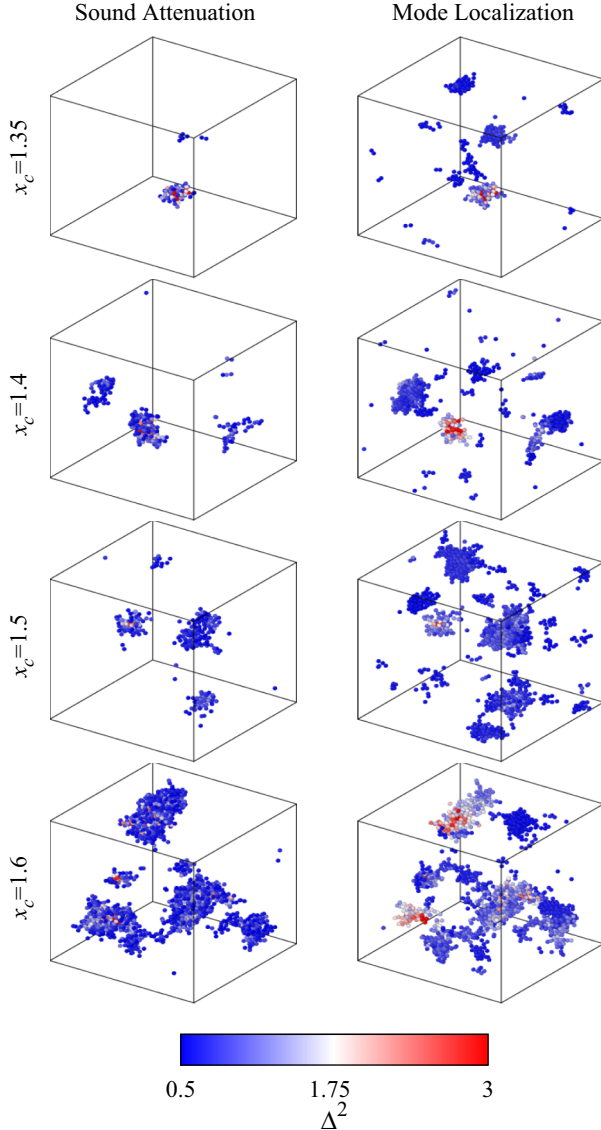
Sound Attenuation   Mode Localization

FIG. 5. The left column illustrates the particles with local phonon attenuation parameter Δ^2 greater than 0.5 at a time corresponding to the period of the excited phonons. Data are averaged over phonons with $n^2 = 1$. The right column illustrates the particles with localized mode participation [Eq. (7)] larger than 5×10^{-5}. Different rows correspond to different interaction potentials, with the interaction range x_c increasing from top to bottom. Particles are color-coded according to their Δ^2 value. The left column demonstrates that scattering defects drive sound attenuation in amorphous materials. The correspondence between the two columns demonstrates that these defects are the quasilocalized vibrational modes.

demonstrates that sound attenuation is promoted by localized regions that identify defects.

This observation poses two questions. One question concerns the relation between the scattering defects and the quasilocalized vibrational modes [17]. The second question concerns the growth dynamics of the nonphononic displacement field. We address these two questions in Secs. V and VII.
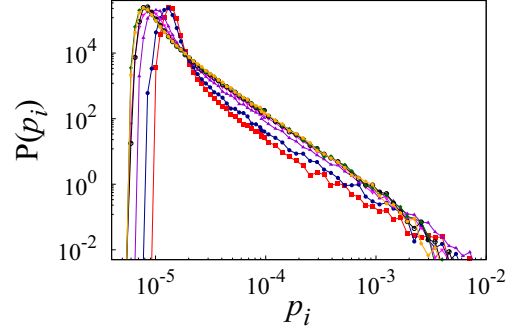

FIG. 6. Probability distribution of the individual particle mode participation p_i^2, for different x_c. The fast decay ($\simeq 1/p_i^2$) reveals that only a small fraction of the particles have large displacements in the low-frequency vibrational modes.

V. SCATTERING DEFECTS AND LOCALIZED VIBRATIONAL MODES

The soft localized regions driving phonon attenuation may be individually apparent as QLMs or may hybridize with extended waves. How many soft regions emerge as QLMs depends on the system size and, possibly, on the stability of the material.

To relate attenuation and vibrational modes we adopt a standard procedure to identify the particles involved in the QLMs [36]. First, we determine the vibrational spectrum via the direct diagonalization of the Hessian matrix $\mathcal{H}_{ij}$ to obtain $k = 1, 2, \ldots$ (normalized) eigenvectors $\mathbf{u}_k$ with associated eigenfrequencies ω_k, $\omega_k \leqslant \omega_{k+1}$. We average the square displacement of particle i in mode k ($\mathbf{u}_{k,i}^2$) over the 0.015% (30) of the eigenmodes with the lowest frequency [36] to define an individual particle participation ratio,

$$p_i = \langle \mathbf{u}_{k,i}^2 \rangle. \tag{7}$$

If particle i only participates in extended modes, then its p_i value is of order $O(1/N)$. Particles with large p_i are those primarily involved in the soft-localized modes. We verified that the number of considered modes is not critical, as p_i is dominated by the contribution of the first few localized modes, with a frequency smaller than that of the boson peak.

We illustrate the probability distribution $P(p_i)$ in Fig. 6. Regardless of the attractive range, the distribution peaks at small p_i values of order $1/N$ and decays approximately as p_i^{-2} at large p_i. The decay of $P(p_i)$ indicates that a few particles have unusually large displacements in the low-frequency modes. The amplitude of $P(p_i)$ at large p_i values depends on x_c, as in short-range attractive potentials (small x_c) localized modes stiffen and shift to higher frequencies, where they hybridize with extended ones [37].

Figure 5 (right column) illustrates the location of the particles with $p_i > 5 \times 10^{-5}$. These particles are arranged into clusters that identify the spatial regions where QLMs localize. The close correspondence between the left and right columns of Fig. 5 suggests QLMs play a key role in the attenuation process.

To have a clearer insight into the influence of the modes on the attenuation process we investigate the $\Delta_i^2(t = T) - p_i$ scatterplot in Figs. 7(a) and 7(b), where Δ_i^2 is measured after
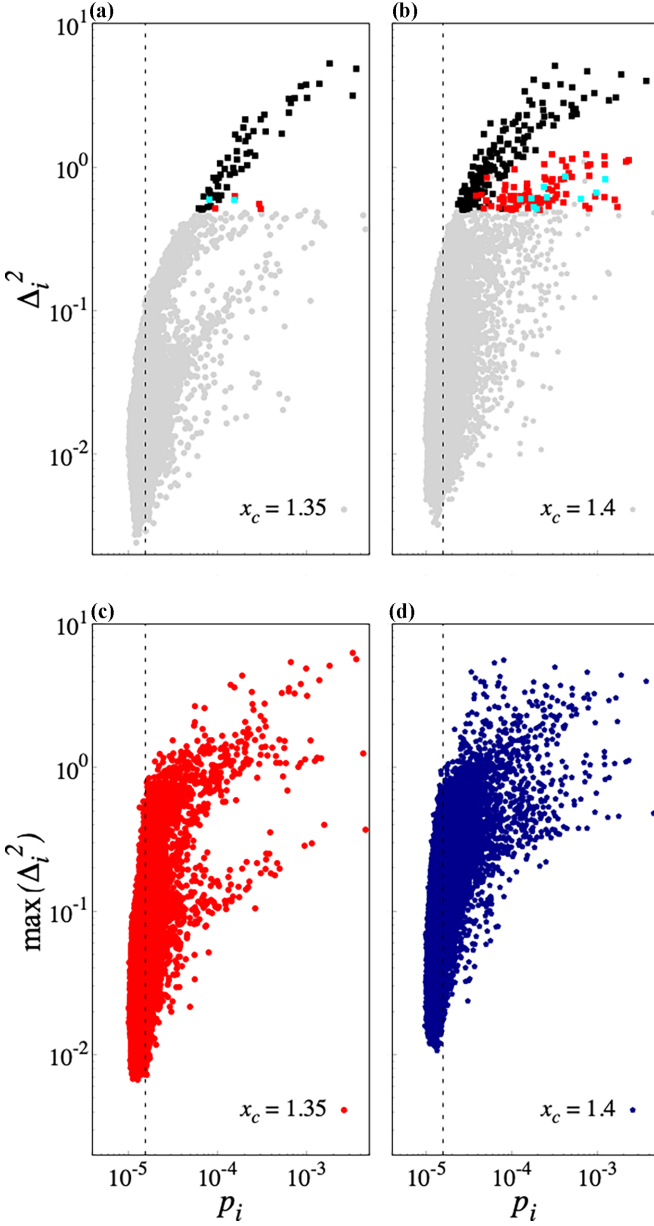
FIG. 7. Scatterplot of the particle attenuation parameter Δ_i^2 against the individual participation ratio p_i for (a) $x_c = 1.35$ and (b) $x_c = 1.4$. Δ_i^2 is evaluated after one period of oscillations for $n = 1$ phonon. Black, red, and cyan points represent particles belonging to the first, second, and third largest clusters illustrated in left column of Fig. 5. (c) and (d) show the corresponding plots obtained by associating with each particle the maximum of Δ_i^2 over the modes with $n = 1$ and $n = 2$. The dashed vertical lines mark the expected p_i value $(1/N)$ for particles only participating in extended modes.

exciting $n = 1$ mode. To interpret this plot, we consider that the particles that contribute most to the attenuation process are those with a large Δ_i^2. These particles may occur in soft regions apparent as individual QLMs, in which case they have large p_i, and in soft regions embedded in extended modes, in which case they have small p_i. Since no particle with a small attenuation coefficient should occur in a soft region, no particle should have a small Δ_i^2 and a large p_i. This prediction is largely supported by Figs. 7(a) and 7(b). We do observe a

few points representing particles with a somehow large value of the participation ratio and a small value of the attenuation parameter, e.g., $p_i \simeq 10^{-3}$ and $\Delta_i^2 \simeq 10^{-2}$. We have found these particles are not involved in the scattering of the considered $n = 1$ phonon but of other ones. Indeed, by associating with each particle the maximum value of Δ_i^2 over the modes with $n = 1$ and 2, we no longer observe particles with a small Δ_i^2 and a large participation ratio, as in Figs. 7(c) and 7(d). These findings echo previous results suggesting that, while quasilocalized modes influence the mechanical properties of amorphous materials, the relevant ones depend on the loading direction [38].

Figure 7 demonstrates the absence of a one-to-one correspondence between Δ_i^2 and p_i. Rather, it suggests different branches depart from the cloud of points with small p_i and Δ_i^2 values. We obtain insights into this organization by performing a cluster analysis of the particles with $\Delta_i^2 > \Delta_c^2$, i.e., the particles visible in Fig. 5 (left column). Two particles are in the same cluster if they are in contact. In Figs. 7(a) and 7(b), we color-code the points representing particles belonging to the three largest clusters in black, red, and cyan and all the others in gray. This study clarifies that the structures in Fig. 7 reflect the particles' organization into distinct clusters. Direct inspection further reveals that, within each cluster, $\Delta_i^2(t)$ is maximal in the center and decays with the radial distance.

VI. MODE CONTRIBUTION

We obtain further insights into the influence of the QLMs on sound attenuation via a normal mode analysis. To this end, we project a phononic displacement field $\mathbf{r}$ on the vibrational mode orthonormal basis $\{\mathbf{u_i}\}$, $\mathbf{r} = \sum a_i\mathbf{u_i}$, $a_i = \mathbf{r} \cdot \mathbf{u_i}$. Exciting this phonon at a time $t = 0$ by imposing appropriate velocities on the particles leads to a velocity field varying in time as $\dot{\mathbf{p}}(t) = \sum a_i\omega_i \cos(\omega_i t)\mathbf{u_i}$, where ω_i is the eigenfrequency of mode i. The associated velocity autocorrelation function is

$$C(t) = \frac{\dot{\mathbf{v}}(t)\dot{\mathbf{v}}(0)}{\dot{\mathbf{v}}(0)\dot{\mathbf{v}}(0)} = \frac{\sum a_i^2\omega_i^2 \cos(\omega_i t)}{\sum a_i^2\omega_i^2}$$

$$\simeq \int P(a^2\omega^2) \cos(\omega t)d\omega. \tag{8}$$

Phonon damping with $C(t) = \cos(\omega_0 t)e^{-\frac{1}{2}\Gamma t}$ then occurs if the probability distribution of $a_i^2\omega_i^2$ is a Lorentzian,

$$P(a^2\omega^2) = \frac{1}{\pi} \frac{\frac{1}{2}\Gamma^2}{\left(\omega - \omega_0^2\right) + \left(\frac{1}{2}\Gamma\right)^2}. \tag{9}$$

Using this projection formalism to investigate sound attenuation does not require knowledge of all the eigenmodes of the Hessian. Rather, one needs the modes contributing to the considered phonon, e.g., enough modes to ensure that $\sum a_i^2$ is approximately 1. Equivalently, one needs the modes with $a_i^2 > 1/dN$ that contribute more than random directions to the phonon in d spatial dimensions. In general, more modes need to be considered as the phonon wavelength decreases. In our $N = 64\,000$ particle systems, we are able to get enough low-frequency modes to reasonably describe $(\sum a_i^2 > 0.96)$ phonons with $n = 1, 2$ for all considered potentials. As an
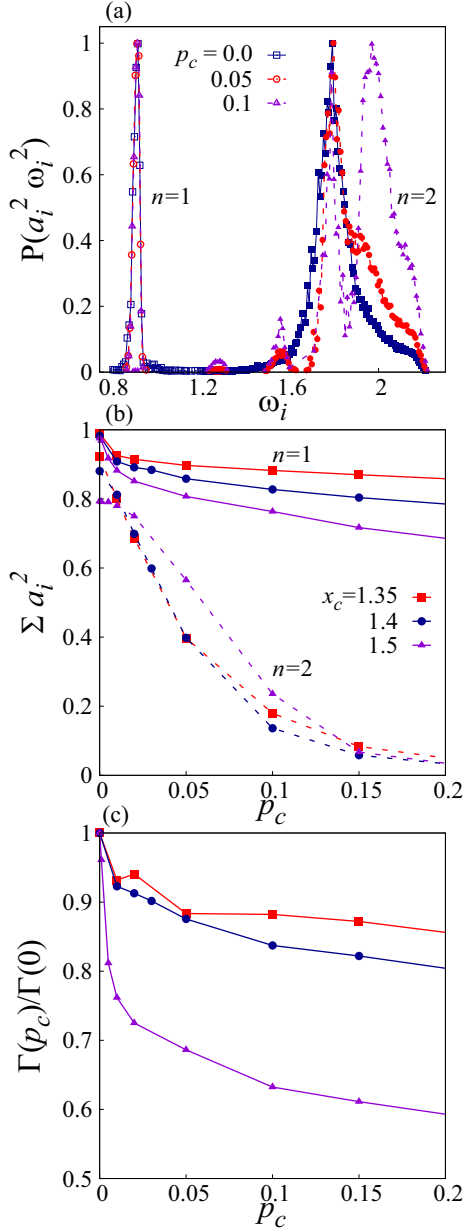
FIG. 8. (a) Probability distribution $P(a^2\omega^2)$ for $x_c = 1.4$ for $n = 1, 2$. The data are averaged over 100 configurations, with 100 underlying phases and $d = 3$ polarizations, considering all modes with participation ratios greater than $p_c = 0, 0.1, 0.2$. (b) The sum of coefficients a_i^2 as a function of threshold p_c. (c) Ratio of Γ_c/Γ_0 as a function of p_c, where Γ_c is the value at finite p_c and Γ_0 represents $p_c = 0$.

example, we illustrate in Fig. 8(a) numerical results for the distribution $P(a^2\omega^2)$ at $x_c = 1.4$. We show results for $n = 1$ (blue open squares) and $n = 2$ (blue solid squares). At each n, the distribution is averaged over 100 phases and 3 polarizations and 100 different samples. The Lorentzian-like shape of this distribution defines an attenuation coefficient which is consistent with that estimated from the decay of the velocity autocorrelation function. Practically, to suppress noise, we obtain Γ from a fit of the cumulative distribution to its

expected functional form, $\frac{1}{2} + \frac{1}{\pi} \arctan(\frac{\omega - \omega_0}{\Gamma})$, focusing on a small range of frequencies close to ω_0.

To assess the influence of soft modes on the attenuation coefficient, we restrict the above analysis to modes with a participation ratio larger than a threshold p_c. Specifically, rather than describing the whole phonon by projecting it on the mode eigenbasis, we consider a fraction of it by projecting on the subspace spanned by the modes with participation ratio $p_i > p_c$. In doing so, we capture a fraction $\sum_{p_i > p_c} a_i^2$ of the exited phonon, as we illustrate in Fig. 8(b), and modify the $P(a^2\omega^2)$ distribution. As an example, Fig. 8(a) shows how the original distributions (blue) change when considering only modes with $p_i \geqslant p_c = 0.05$ (red) and $\geqslant 0.1$ (magenta). From this analysis, we are able to extract a p_c-dependent sound attenuation coefficient $\Gamma(p_c)$, which is interpreted as the attenuation coefficient obtained after filtering out the influence of the modes with participation smaller than p_c.

We start by describing $n = 1$ phonon. For $n = 1$, $\sum a_i^2$ drops gently as p_c increases, as illustrated in Fig. 8(b), indicating that the phonons have a minimal projection on the localized modes. Nevertheless, the removal of this minimal projection influences the attenuation rate, as in Fig. 8(c). The result is particularly apparent for $x_c = 1.5$, whose vibrational properties have similarities to a poorly annealed glass [17]. Henceforth, in this considered case, QLMs act as scattering sources at short times and sensibly influence the attenuation coefficient.

The QLMs' influence is more dramatic for $n = 2$. In this case, $\sum a_i^2$ sensibly drops with p_c, as in Fig. 8(b), and $P(a^2\omega^2)$ strongly depends on p_c, as in Fig. 8(a). These results imply the modes with a small participation ratio critically influence the modes with $n = 2$ and their attenuation coefficient. These modes influence $P(a^2\omega^2)$ so strongly that it can no longer be reasonably approximated by a Lorentzian. Henceforth, the p_c dependence of the damping coefficient is ill defined, which is why we do not illustrate $\Gamma(p_c)$ in Fig. 8(c).

VII. SOUND ATTENUATION SPATIOTEMPORAL DYNAMICS

We investigate the spatiotemporal evolution of the local sound attenuation parameter in Fig. 9 by illustrating the particles with $\Delta_i^2 > \Delta_c^2$ at times corresponding to one, two, three, and four oscillation periods, from top to bottom, for $x_c = 1.4$ (left column) and $x_c = 1.6$ (right). The difference in the two columns reflects the interaction potential dependence of the attenuation parameter Γ. Since $\Gamma(x_c = 1.6) \simeq 3\Gamma(x_c = 1.4)$, more particles have $\Delta_i^2 > \Delta_c^2$ for $x_c = 1.6$ than for $x_c = 1.4$ after four oscillation periods. Figure 9 reveals that attenuation proceeds through the growth of the clusters of attenuated particles observed at early times, rather than via the emergence of disconnected clusters.

We quantify this growth process by studying the time dependence of the total number of particles with $\Delta_i^2 > \Delta_c^2$, N_Δ, and of the linear size of the largest cluster, $\lambda = (N_L/\rho)^{1/3}$, with N_L being the number of particles in the cluster. Figures 10(a) and 10(b) show that, at early times, $\lambda^2 \propto t/\tau$, and $N_\Delta \propto (t/\tau)^{3/2}$. While attenuation in the harmonic regime we are investigating is deterministic as determined by the dephasing of the excited modes, Eq. (8), these findings are
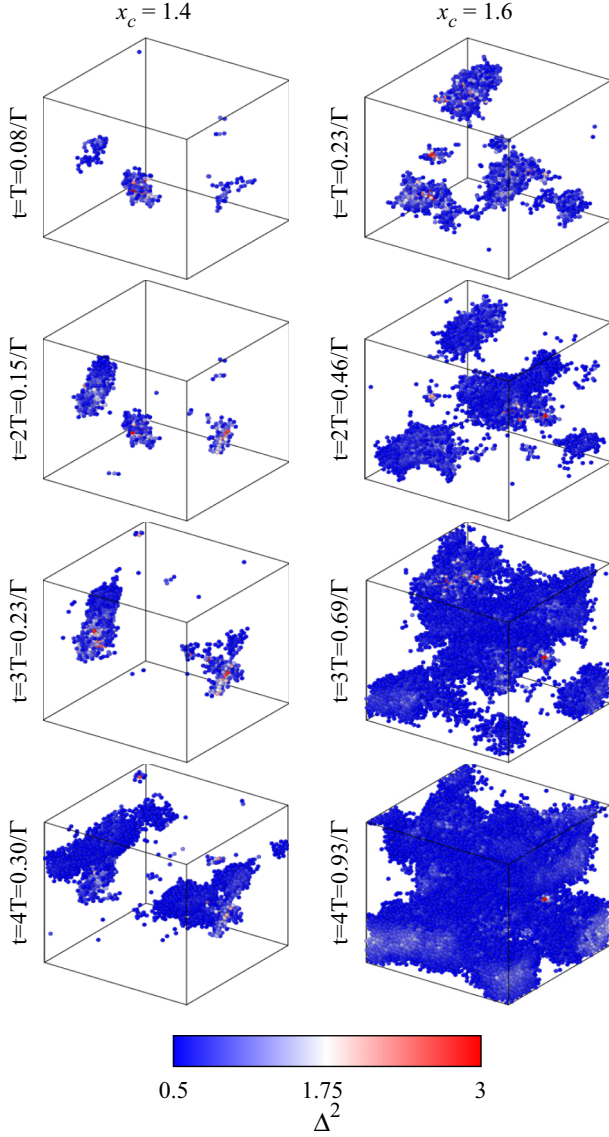
FIG. 9. Particles with local phonon attenuation parameter $\Delta^2 > 0.5$ after one, two, three, and four phonon oscillation periods for $x_c = 1.4$ (left) and 1.6 (right).
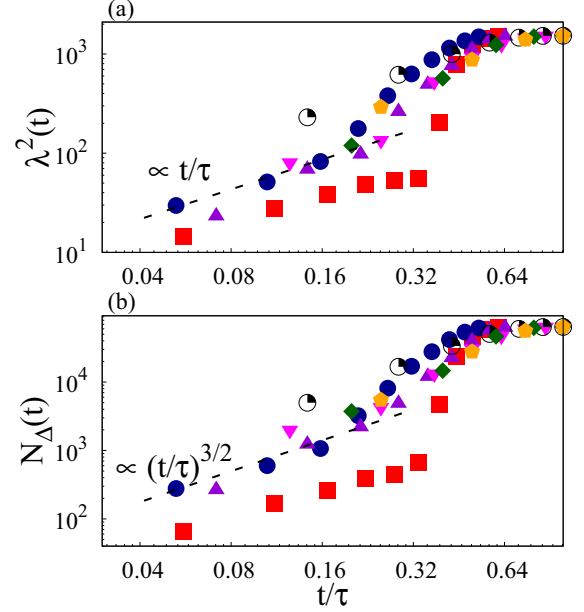

FIG. 10. Time dependence of the square linear size λ^2 of the largest cluster of particles with local damping parameter $\Delta_i^2(t) > 0.5$ and of the overall number of particles with $\Delta_i^2(t) > 0.5$. The early time growth of these quantities shows that the nonphononic field propagates via a diffusive process. These quantities grow quickly at later times, as the peak of the $P(\Delta_i^2(t))$ distribution approaches the considered threshold value of 0.5.

compatible with a picture according to which the local attenuation parameter field $\Delta^2(\mathbf{r})$ is localized in a few regions at very early times and then spreads through a diffusive process.

At later times, both λ^2 and N_Δ grow sharply. This fast growth reflects the time dependence of the $P(\Delta_i^2)$ distribution, which we illustrated in Fig. 6. This distribution peaks at a Δ_i^2 value that increases with time. λ and N_Δ grow sharply as the central peak approaches the threshold value Δ_c we used to identify the attenuated particles. Indeed, we observe the time of this fast growth depends on the chosen threshold.

VIII. CONCLUSIONS

We resolved phonon attenuation in space and time in the Rayleigh scattering regime in three-dimensional model amorphous solids. To do this, we introduced a nonphononic displacement field measuring the difference between the actual displacement of the particles and what it would be in the absence of attenuation. The spatiotemporal evolution of this field reveals that attenuation begins in specific localized defects and then spreads diffusively throughout the material. These localized defects indicate softer areas within the system and often overlap with regions where low-frequency vibrational modes are concentrated. Overall, these results support a picture according to which scattering by localized defects drives the attenuation of sound waves in three-dimensional amorphous materials.

Previous works suggesting that QLMs drive sound attenuation in three-dimensional amorphous solids captured the dependence of the attenuation parameter on material properties [17] but were quantitatively inaccurate [7]. Our results suggest this could occur because the defects inducing attenuation are not all apparent as individual QLMs. Rather, the fraction of defects apparent as QLMs is expected to decrease with the system size due to their increased hybridization with extended waves. In large systems, other techniques might possibly be employed to identify localized soft regions [39]. Relating sound attenuation to the properties of these regions is an interesting avenue of research that could benefit from previous approaches used to describe how the heterogeneities in the size of the grain boundaries affect sound attenuation in polycrystals [40].

One of the most interesting future research avenues concerns the study of the dimensionality dependence of the attenuation process. In three dimensions, the few investigations of sound attenuation conducted so far suggest that the attenuation coefficient scales with material properties as

predicted by correlated fluctuating elasticity [34], $\Gamma/\omega_0 \propto \xi^3 \gamma(\omega/\omega_0)^4$, with ξ being the shear modulus's spatial correlation length. Conversely, in two dimensions, previous results supported [9,33] the FET scenario [10,11], $\Gamma/\omega_0 \propto \gamma(\omega/\omega_0)^3$. In addition, in two dimensions, QLMs appear to be irrelevant [35] because they strongly hybridize with plane waves [41] and disappear in large enough systems [18,35]. The two- and three-dimensional scenarios may be compatible if the correlation length ξ, which depends on the material properties in three dimensions, is weakly dependent on them in two dimensions, as we observed in a model system [42], so that the corr-FET prediction reduces to the FET one. Alternatively, the defect picture may be relevant in three dimensions, not two. In this respect, it is worth noticing that size effects on sound attenuation are much stronger in two [31] than in three dimensions [18,32]. This question might be addressed by investigating the nonphononic field in two-dimensional systems.

Our findings highlight a similarity between the behavior of sound attenuation and the dynamical heterogeneities observed in supercooled liquids [43]. In the case of phonon attenuation, we observed that particles with an attenuation parameter exceeding a certain threshold initially localize in specific regions, which gradually expand over time to encompass the entire system. Likewise, in supercooled liquids, particles that move beyond a microscopic threshold during relaxation also localize in specific regions that grow over time and eventually encompass the entire system. Furthermore, as we have found attenuation correlates with QLMs, relaxation has been shown to correlate with QLMs [36]. Since sound attenuation occurs in the linear response regime, this analogy indicates that dynamical heterogeneities may have a reversible component associated with particles' vibrations. It explains why they are not an optimal proxy of structural relaxation [44,45].

[1] C. Masciovecchio, G. Baldi, S. Caponi, L. Comez, S. Di Fonzo, D. Fioretto, A. Fontana, A. Gessini, S. C. Santucci, F. Sette, G. Viliani, P. Vilmercati, and G. Ruocco, Evidence for a crossover in the frequency dependence of the acoustic attenuation in vitreous silica, Phys. Rev. Lett. **97**, 035501 (2006).

[2] G. Baldi, V. M. Giordano, G. Monaco, and B. Ruta, Sound attenuation at terahertz frequencies and the boson peak of vitreous silica, Phys. Rev. Lett. **104**, 195501 (2010).

[3] G. Monaco and V. M. Giordano, Breakdown of the Debye approximation for the acoustic modes with nanometric wavelengths in glasses, Proc. Natl. Acad. Sci. U.S.A. **106**, 3659 (2009).

[4] B. Ruta, G. Baldi, F. Scarponi, D. Fioretto, V. M. Giordano, and G. Monaco, Acoustic excitations in glassy sorbitol and their relation with the fragility and the boson peak, J. Chem. Phys. **137**, 214502 (2012).

[5] G. Baldi, M. Zanatta, E. Gilioli, V. Milman, K. Refson, B. Wehinger, B. Winkler, A. Fontana, and G. Monaco, Emergence of crystal-like atomic dynamics in glasses at the nanometer scale, Phys. Rev. Lett. **110**, 185503 (2013).

[6] H. Mizuno, G. Ruocco, and S. Mossa, Sound damping in glasses: Interplay between anharmonicities and elastic heterogeneities, Phys. Rev. B **101**, 174206 (2020).

[7] G. Szamel and E. Flenner, Microscopic analysis of sound attenuation in low-temperature amorphous solids reveals quantitative importance of non-affine effects, J. Chem. Phys. **156**, 144502 (2022).

[8] M. Baggioli and A. Zaccone, Theory of sound attenuation in amorphous solids from nonaffine motions, J. Phys.: Condens. Matter **34**, 215401 (2022).

[9] W. Schirmacher, G. Ruocco, and T. Scopigno, Acoustic attenuation in glasses and its relation with the boson peak, Phys. Rev. Lett. **98**, 025501 (2007).

[10] W. Schirmacher, Thermal conductivity of glassy materials and the "boson peak," Europhys. Lett. **73**, 892 (2006).

[11] A. Marruzzo, W. Schirmacher, A. Fratalocchi, and G. Ruocco, Heterogeneous shear elasticity of glasses: The origin of the boson peak, Sci. Rep. **3**, 1407 (2013).

[12] S. R. Elliott, A unified model for the low-energy vibrational behaviour of amorphous solids, Europhys. Lett. **19**, 201 (1992).

[13] J. E. Graebner, B. Golding, and L. C. Allen, Phonon localization in glasses, Phys. Rev. B **34**, 5696 (1986).

[14] J. Kawahara, Scattering attenuation of elastic waves due to low-contrast inclusions, Wave Motion **48**, 290 (2011).

[15] G. Kapteijns, D. Richard, E. Bouchbinder, and E. Lerner, Elastic moduli fluctuations predict wave attenuation rates in glasses, J. Chem. Phys. **154**, 081101 (2021).

[16] J. W. Strutt (Lord Rayleigh), On the transmission of light through an atmosphere containing small particles in suspension, and on the origin of the blue of the sky, Philos. Mag. **47**, 375 (1903).

[17] S. Mahajan and M. P. Ciamarra, Unifying description of the vibrational anomalies of amorphous materials, Phys. Rev. Lett. **127**, 215504 (2021).

[18] H. Mizuno, H. Shiba, and A. Ikeda, Continuum limit of the vibrational properties of amorphous solids, Proc. Natl. Acad. Sci. U.S.A. **114**, E9767 (2017).

[19] G. Kapteijns, E. Bouchbinder, and E. Lerner, Universal nonphononic density of states in 2D, 3D, and 4D glasses, Phys. Rev. Lett. **121**, 055501 (2018).

[20] U. Buchenau, Y. M. Galperin, V. L. Gurevich, D. A. Parshin, M. A. Ramost, and H. R. Schober, Interaction of soft modes and sound waves in glasses, Phys. Rev. B **46**, 2798 (1992).

[21] B. Rufflé, D. A. Parshin, E. Courtens, and R. Vacher, Boson peak and its relation to acoustic attenuation in glasses, Phys. Rev. Lett. **100**, 015501 (2008).

[22] H. Mizuno, S. Mossa, and J.-L. Barrat, Acoustic excitations and elastic heterogeneities in disordered solids, Proc. Natl. Acad. Sci. U.S.A. **111**, 11949 (2014).

[23] D. Richard, K. González-López, G. Kapteijns, R. Pater, T. Vaknin, E. Bouchbinder, and E. Lerner, Universality of the nonphononic vibrational spectrum across different classes of computer glasses, Phys. Rev. Lett. **125**, 085502 (2020).

[24] C. Rainone, E. Bouchbinder, and E. Lerner, Pinching a glass reveals key properties of its soft spots, Proc. Natl. Acad. Sci. U.S.A. **117**, 5228 (2020).

[25] O. Dauchot, S. Karmakar, I. Procaccia, and J. Zylberg, Athermal brittle-to-ductile transition in amorphous solids, Phys. Rev. E **84**, 046105 (2011).

[26] J. Chattoraj and M. P. Ciamarra, Role of attractive forces in the relaxation dynamics of supercooled liquids, Phys. Rev. Lett. **124**, 028001 (2020).

[27] K. González-López, M. Shivam, Y. Zheng, M. P. Ciamarra, and E. Lerner, Mechanical disorder of sticky-sphere glasses. I. Effect of attractive interactions, Phys. Rev. E **103**, 022605 (2021).

[28] K. González-López, M. Shivam, Y. Zheng, M. P. Ciamarra, and E. Lerner, Mechanical disorder of sticky-sphere glasses. II. Thermomechanical inannealability, Phys. Rev. E **103**, 022606 (2021).

[29] Y. Zheng, S. Mahajan, J. Chattoraj, and M. Pica Ciamarra, Designing phononic band gaps with sticky potentials, Front. Phys. **9**, 665391 (2021).

[30] R. Fletcher, *Numerical Analysis* (Springer, Berlin, 1976), pp. 73–89.

[31] S. Gelin, H. Tanaka, and A. Lematre, Anomalous phonon scattering and elastic correlations in amorphous solids, Nat. Mater. **15**, 1177 (2016).

[32] H. Mizuno and A. Ikeda, Phonon transport and vibrational excitations in amorphous solids, Phys. Rev. E **98**, 062612 (2018).

[33] E. Maurer and W. Schirmacher, Local oscillators vs elastic disorder: A comparison of two models for the boson peak, J. Low Temp. Phys. **137**, 453 (2004).

[34] W. Schirmacher, Some comments on fluctuating-elasticity and local oscillator models for anomalous vibrational excitations in glasses, J. Non-Cryst. Solids **357**, 518 (2011).

[35] C. Caroli and A. Lemaître, Key role of retardation and non-locality in sound propagation in amorphous solids as evidenced by a projection formalism, J. Chem. Phys. **153**, 144502 (2020).

[36] A. Widmer-Cooper, H. Perry, P. Harrowell, and D. R. Reichman, Irreversible reorganization in a supercooled liquid originates from localized soft modes, Nat. Phys. **4**, 711 (2008).

[37] E. Lerner and E. Bouchbinder, Boson-peak vibrational modes in glasses feature hybridized phononic and quasilocalized excitations, J. Chem. Phys. **158**, 194503 (2023).

[38] J. Ding, S. Patinet, M. L. Falk, Y. Cheng, and E. Ma, Soft spots and their structural signature in a metallic glass, Proc. Natl. Acad. Sci. U.S.A. **111**, 14052 (2014).

[39] D. Richard, G. Kapteijns, and E. Lerner, Detecting low-energy quasilocalized excitations in computer glasses, Phys. Rev. E **108**, 044124 (2023).

[40] A. P. Arguelles and J. A. Turner, Ultrasonic attenuation of polycrystalline materials with a distribution of grain sizes, J. Acoust. Soc. Am. **141**, 4347 (2017).

[41] E. Bouchbinder and E. Lerner, Universal disorder-induced broadening of phonon bands: From disordered lattices to glasses, New J. Phys. **20**, 073022 (2018).

[42] S. Mahajan and M. P. Ciamarra, Quasi-localized vibrational modes, boson peak and sound attenuation in model mass-spring networks, SciPost Phys. **15**, 069 (2023).

[43] L. Berthier, G. Biroli, J.-P. Bouchaud, L. Cipelletti, and W. van Saarloos, in *Dynamical Heterogeneities in Glasses, Colloids, and Granular Media*, edited by L. Berthier (Oxford University Press, Oxford, 2011), p. 450.

[44] R. L. Jack, A. J. Dunleavy, and C. P. Royall, Information-theoretic measurements of coupling between structure and dynamics in glass formers, Phys. Rev. Lett. **113**, 095703 (2014).

[45] Y.-W. Li, Y. Yao, and M. P. Ciamarra, Local plastic response and slow heterogeneous dynamics of supercooled liquids, Phys. Rev. Lett. **128**, 258001 (2022).